Biosensors and Bioelectronics 24 (2009) 3448–3454

Contents lists available at ScienceDirect

Biosensors and Bioelectronics

journal homepage: www.elsevier.com/locate/bios

Nanoplated bismuth titanate sub-microspheres for protein immobilization and their corresponding direct electrochemistry and electrocatalysis

Xiaohua Chen [a], Jianqiang Hu [a,**], Zhiwu Chen [b], Xiumei Feng [a], Aiqing Li [c,*]

[a] College of Chemistry and Chemical Engineering, South China University of Technology, Guangzhou 510640, PR China
[b] College of Materials Science and Engineering, South China University of Technology, Guangzhou 510640, PR China
[c] College of Medicine & Public Health, The Ohio State University, Columbus, OH 43210, USA

ARTICLE INFO

Article history:
Received 15 February 2009
Received in revised form 11 April 2009
Accepted 24 April 2009
Available online 3 May 2009

Keywords:
Direct electrochemistry
Electrocatalysis
$Bi_4Ti_3O_{12}$ sub-microspheres
Hemoglobin
Hydrogen bond and electrostatic assembly
Biosensor

ABSTRACT

A layered inorganic perovskite sub-micrometer-scale material, nanoplated bismuth titanate ($Bi_4Ti_3O_{12}$) sub-microspheres (NBTSMs) constructed with tens of $Bi_4Ti_3O_{12}$ nanoplates, was for the first time synthesized by a facile hydrothermal synthesis strategy. The NBTSMs were employed as a supporting matrix to explore a novel immobilization and biosensing platform of redox proteins through a combined hydrogen bond and electrostatic assembly process. Biocompatibility, stability, reproducibility, and electrochemical and electrocatalytic properties of the resulting NBTSMs-based composite were studied by UV–vis absorption, FTIR, and electrochemical methods. The research results revealed that the NBTSMs-based composite was a satisfying matrix for proteins to effectively retain their native structure and bioactivity. With advantages of the $Bi_4Ti_3O_{12}$ layered material, facilitated direct electron transfer of the metalloenzymes with an apparent heterogeneous electron transfer rate constant (k_s) of $20.0 \pm 3.8\ s^{-1}$ was acquired on the NBTSMs-based enzyme electrode. The NBTSMs-based biosensor demonstrated significant electrocatalytic activity for the reduction of hydrogen peroxide with an apparent Michaelis–Menten constant (204 μM), wide linear range (2–430 μM), and low detection limit (0.46 μM, S/N = 3). These indicated that the nanoplate-constructed $Bi_4Ti_3O_{12}$ sub-microspheres were one of ideal candidate materials for direct electrochemistry of redox proteins and the construction of the related enzyme biosensors, and may find potential applications in biomedical, food, and environmental analysis and detection.

1. Introduction

Direct electrochemistry of redox proteins constructed on nanomaterials has recently attracted considerable attention from electrochemical scientists because it can not only serve as an ideal model to understand electron transfer mechanisms in biological systems (Armstrong et al., 1988; Wang, 2008), but also offer great potential for use in many fields such as the construction of third-generation biosensors (Jia et al., 2002), enzyme biofuel cells (Ivnitski et al., 2006), biosensing (Cai et al., 2008), biocatalysis (Zhang et al., 2007), biodetection (Pal et al., 2007), and protein identification (Rinehart et al., 2007). However, it is difficult for proteins to realize direct electron transfer on "bare" electrodes because of their easy denaturation, deeply embedded active centers, and often unfavorable orientations (Heller, 1990; Liu et al., 2005). The aim to construct an electrochemical biosensor involves protein immobilization onto an electrode surface and efficient electron communication between the protein and the underlying electrode while retaining the protein stability and bioactivity. To maintain or acquire native structures and appropriate orientations of redox proteins and an increased electron transfer ability between the proteins and the electrodes, variously supporting matrices have been explored for the construction of biosensors, such as surfactant (Wang et al., 2007), polymer (Li et al., 2007), sol–gel (Di et al., 2007), and nanomaterial (Zhang and Oyama, 2005; Du et al., 2007). Recent promising work in this field is to employ nanostructured materials for the fabrication of biosensors because nanomaterials possess high surface-volume ratio and unique physical and chemical properties (Willner et al., 2007; Lu et al., 2008). Many efforts have been made to date for designing novel sensing systems and enhancing electrochemical performance of such biosensors through tailoring the component, size, structure, and shape of nanomaterials (Zhang and Oyama, 2005; Du et al., 2007).

At present, metal, semiconductor, and magnetic nanomaterials have been extensively utilized to build electrochemical biosensors (Xu et al., 2007a; Guo et al., 2008; Cheng et al., 2005). However, to the best of our knowledge, fabrication and direct electrochemistry study of biosensors based on inorganic perovskite nanomaterials are rarely reported to date although some inorganic nanomaterials

* Corresponding author. Tel.: +1 614 292 4420; fax: +1 614 688 8742.
** Corresponding author. Tel.: +86 20 222 36670; fax: +86 20 222 36670.
E-mail addresses: jqhusc@scut.edu.cn (J. Hu), li.586@osu.edu (A. Li).

0956-5663/$ – see front matter © 2009 Elsevier B.V. All rights reserved.
doi:10.1016/j.bios.2009.04.037

have also been used to construct biosensors and direct electrochemistry studies (Zhang et al., 2007; Qiao et al., 2008). Very interestingly, it is much easy for inorganic ferroelectric nanomaterials to form layered structures (Yang et al., 2003). Recently, the layered porous nanostructures with flexible pore sizes and shapes are attracting considerable interest in bioanalytical area because the layered porous matrix permits access to the bound enzymes. For example, Zhang et al. (2007) has reported that the composite of Mb intercalated into layered nanosheets was useful as biocatalysts, which possessed an excellent catalytic performance and much high stability. Previous studies also showed that layered porous inorganic nanomaterials could not only maintain the activity of the bound proteins but also improve their stability.

Bismuth titanate ($Bi_4Ti_3O_{12}$) possessing layered perovskite structure is built up by the regular intergrowth of $[Bi_2O_2]^{2+}$ layer and perovskite type layers $[Bi_2Ti_3O_{10}]^{2-}$ where Bi ions occupy twelve-coordinated sites (Yang et al., 2003). As a typical ferroelectric, piezoelectric and electro-optic material, $Bi_4Ti_3O_{12}$ has relatively low coercive field, low dielectric constant, high Curie temperature, high breakdown strength, and high electrical conductivity anisotropy characters (Villegas et al., 1996). Moreover, $Bi_4Ti_3O_{12}$ exhibits potential use in many areas such as non-volatile memory, optical memory, and piezoelectric and electro-optic devices. Both the unique structure and properties of the $Bi_4Ti_3O_{12}$ nanomaterials are reasonably expected to construct promising electrochemical biosensors. In the present work, we synthesized nanoplated bismuth titanate sub-microspheres (NBTSMs) by a facile hydrothermal synthesis strategy. The NBTSMs were combined with heme protein to fabricate electrochemical biosensor by a combined hydrogen bond and electrostatic assembly methodology. Without introducing any cross-linking reagents, the NBTSMs could well reserve their native layered structure and properties to a large extent, and facilitated direct electron transfer of hemoglobin (Hb) entrapped in the NBTSMs has been acquired. The prepared biosensor was successfully employed for the detection of hydrogen peroxide (H_2O_2) and displayed good performance.

2. Materials and methods

2.1. Chemicals and reagents

Hemoglobin (Hb, from bovine blood) and chitosan (Chi) were purchased from Sigma. Other chemical reagents such as bismuth nitrate, titanium dioxide, hydrogen peroxide, nitric acid, oxalic acid, sodium dihydrogen phosphate, disodium hydrogen phosphate, potassium chloride, potassium ferricyanide, potassium ferrocyanide, sodium hydroxide, phosphoric acid, and high pure nitrogen gas were obtained from Guangdong Guanghua Chemical Reagent Company. All above reagents were analytical grade and used without further purification. Phosphate buffer solutions (PBS, 20 mM) with various pH values were prepared by mixing stock standard solutions and adjusting the pH with a small quantity of sodium hydroxide or phosphoric acid. All aqueous solutions were prepared with Milli-Q purified water (>18.0 MΩ cm).

2.2. Apparatus and measurements

Scanning electron microscopy (SEM) and energy-dispersive X-ray spectroscopy (EDS) were performed with a field-emission microscope (LEO, 1530 VP) operated at an accelerating voltage of 30 kV. Powder X-ray diffraction (XRD) pattern was recorded on a powder sample using a D/max-IIIA (Japan) X-ray diffractometer with Cu Kα radiation (λ = 0.15418 nm). UV–visible (UV–vis) absorption spectroscopy measurement was carried out with a U-3010 spectrophotometer (Hitachi, Japan). Fourier-transform infrared (FTIR) spectra were obtained on Tensor 27 (Bruker Company, German). Electrochemical impedance spectroscopy (EIS) spectra were acquired using an AUTOLAB advanced electrochemical system (Swiss). Electrochemical experiments were carried out at room temperature using a CHI 660 electrochemical workstation (CH Instruments, Inc., Austin, USA). All electrochemical measurements were based on a three-electrode system with the film electrode as working electrode, an Ag/AgCl (3 M KCl) electrode as reference electrode, and a platinum wire as auxiliary electrode, respectively. Without special statement, 20 mM pH 7.0 PBS was used as the electrolyte in all experiments.

2.3. Synthesis of nanoplated bismuth titanate sub-microspheres (NBTSMs)

In a typical procedure for the synthesis of NBTSMs, $Bi(NO_3)_3{\cdot}5H_2O$ (1.6298 g) and TiO_2 (0.192 g) were added respectively to 80 mL 2.5 M NaOH and kept stirring for 3 h to form a homogeneous solution. The mixture was then put into a 100 mL Teflon-lined stainless-steel autoclave. The final product was obtained by heating the autoclave at 160 °C for 48 h, repeatedly washing with milli-Q water, and drying at 80 °C for 4 h while the autoclave was cooled to room temperature.

2.4. Preparation of different modified electrodes

Glassy carbon (GC) electrode was first polished with alumina slurry of successively smaller particles (1.0, 0.3, and 0.05 μm diameters), respectively. Then, the electrode was cleaned by ultrasonication. Finally, the cleaned GC electrode was activated through oxidizing the electrode surface at 1.8 V for 3 min and then reducing it at −1.5 V for 1 min in 0.1 M HNO_3. In addition, to acquire optimum cyclic voltammetric responses of the Hb-NBTSMs/GC, the control experiments of NBTSMs concentrations were performed (Fig. S1), indicating that the optimum concentration was 1 mg/mL. In a typical procedure for the preparation of Hb-NBTSMs modified electrode, 5 μL of 2 mg/mL NBTSMs PBS was first cast onto the activated GC electrode surface for the hydrogen bond formation between the electrode and NBTSMs. After 10 min, an equal volume of 4 mg/mL Hb PBS was again cast onto the electrode surface to self-assemble between positively charged NBTSMs and negatively charged Hb. Finally, a uniform film electrode was formed through putting the as-prepared electrode overnight at room temperature, and then used for electrochemical investigations or stored at 4 °C in a refrigerator when not in use.

For comparison, Hb-Chi-NBTSMs/GC and NBTSMs/GC electrodes were also prepared. The suspension containing 2 mg/mL Hb, 1 mg/mL Chi and 1 mg/mL NBTSMs was used to construct the Hb-Chi-NBTSMs/GC electrode while 1 mg/mL NBTSMs solution was employed to fabricate the NBTSMs/GC electrode.

3. Results and discussion

3.1. Morphology and structure characterization of the NBTSMs

Fig. 1 shows SEM images of the as-prepared NBTSMs. The NBTSMs possessed an average diameter of about 610 nm while its comprising nanoplates had the thickness and side length of about 60 and 440 nm, respectively. It can be clearly seen that tens of the nanoplates intercalated together from the magnified SEM image (Fig. 1B). Such intercalated structure not only offered higher surface area but also had numerous nanometer-scale cavities and highly active sites, which were much useful for proteins to sequester in the cavities or bind on the surface.

To verify the component of the sample produced thus, EDS measurement was preformed. The Cu, C, Au, and Pd elements (Fig. S2)

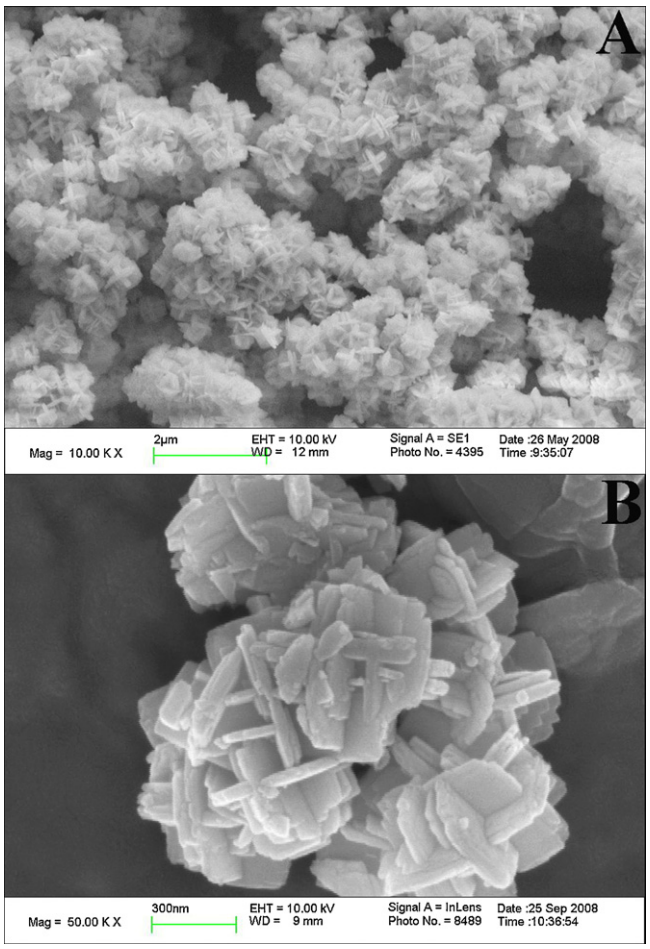

Fig. 1. SEM images of the NBTSMs prepared using the present method.

were from the copper grids and spurted Au–Pd alloy made for the SEM sample. The appearance of three elements of Bi, Ti, and O indicated that the sample was probably $Bi_4Ti_3O_{12}$. Then, XRD measurement was used to ascertain the sample component. The diffraction peaks of 21.7°, 23.3°, 30.45°, 32.8°, 39.7°, 47.1°, 52.4°, and 57.1° could be indexed to (0 8 0), (1 1 1), (1 7 1), (2 0 0), (2 8 0), (2 0 2), (2 8 2), and (1 7 3) planes of the orthorhombic structure of bismuth titanate (JCPDS: 35-0795), respectively (Fig. S3). No characteristic peaks of impurities such as Bi_2O_3 and TiO_2 were observed, indicating that the sample was pure $Bi_4Ti_3O_{12}$.

3.2. Self-assembly and spectroscopic analysis of Hb-NBTSMs/GC composite film

The Hb-NBTSMs composite film on the activated GC electrode was acquired through a hydrogen bond and electrostatic self-assembly process, as illustrated in Fig. 2. The cleaned GC electrode was first activated at diluted nitric acid through cyclic voltammetry method. Previous studies have demonstrated that the electrochemically treated GC surface possesses microporous structure (Nagaoka and Yoshino, 1986) and contains functional groups of –COOH, –COH, $-C_6H_5OH$, –OH, etc. (Shi et al., 2007). Consequently, the NBTSMs possessing sub-micrometer-scale size and copious oxygen atoms easily self-assembled onto the activated electrode through hydrogen bond when the NBTSMs PBS was added (Fig. S4). The formation mechanism of the hydrogen bond was consistent with that previously reported (Wang et al., 2002). The electrophoresis measurement (Fig. S5) documented that the NBTSMs were positively charged with electricity. Therefore, introducing negatively charged Hb (isoelectric point was about 6.8) in pH 7.0 PBS on the surface of the as-prepared electrode, multi-layer self-assembly film containing NBTSMs and Hb was obtained through electrostatic attraction (Chen et al., 2008).

To evaluate the self-assembly process and interfacial electron transfer property of the Hb-NBTSMs modified electrode, EIS was preformed. Previous studies have proved that the impedance spectrum involving a semicircle portion at high frequencies corresponds to the electron transfer limiting process (Pei et al., 2001), using which the electron transfer resistance (Rct) can be gained by measuring its diameter. When a bare GC electrode was activated, its transfer resistance (Rct) could be estimated to be about 480 Ω (curve a in Fig. S6). But, when the NBTSMs self-assembled onto the electrode, a small increase of the interfacial resistance (about 890 Ω) was observed (curve b in Fig. S6), which was probably due to the spatial resistance between NBTSMs and the

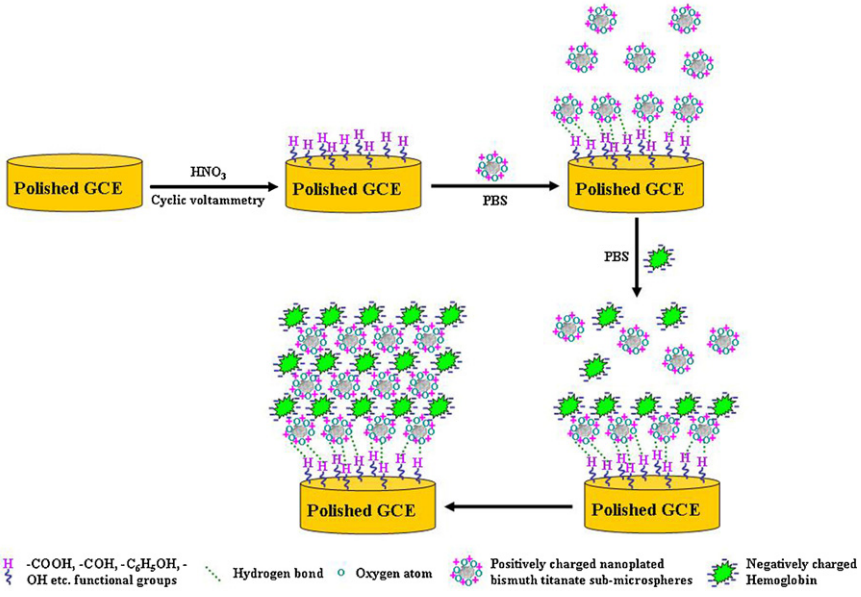

Fig. 2. Schematic illustration of the self-assembly of the NBTSMs and Hb on the activated GC electrode through hydrogen bond and electrostatic attraction.

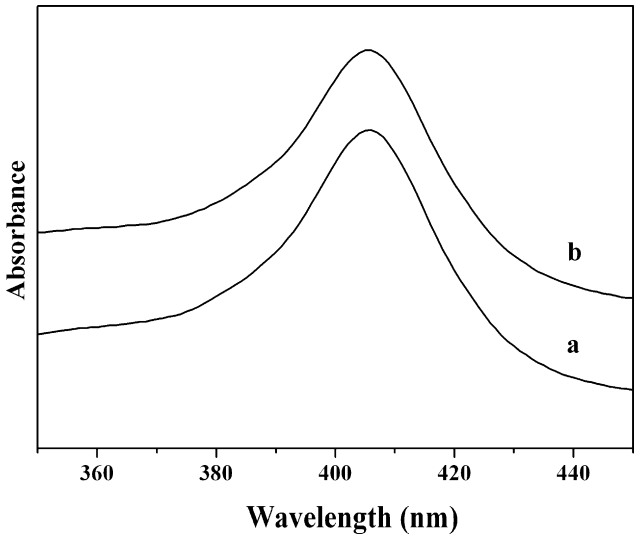

Fig. 3. UV–vis spectra of dry (a) Hb and (b) Hb-NBTSMs films.

probe molecule, $Fe(CN)_6^{3-/4-}$. With further introducing Hb onto the NBTSMs electrode, negatively charged Hb orderly assembled onto the positive electrode surface through electrostatic attraction, which was demonstrated by the tremendous increase resistance (about 3300 Ω) at the Hb-NBTSMs electrode (curve c in Fig. S6). The great interfacial resistance also indicated that Hb hindering electron transfer pathway was successfully immobilized on the surface of the Hb-NBTSMs electrode.

3.3. UV–vis and FTIR spectroscopic characterizations of Hb-NBTSMs composite film

Fig. 3 shows UV–vis absorption spectra of dry Hb and Hb-NBTSMs films. An obvious UV–vis absorption peak at around 405 nm from dry Hb film could be clearly discerned, which was a characteristic Soret absorption bands (curve a). When Hb was entrapped in the NBTSMs films, the position and intensity of the Hb spectrum peak were similar to that of pure Hb film (curve b), suggesting that the Hb retained the essential features of its native secondary structure in the Hb-NBTSMs composite film and had good biocompatibility with the NBTSMs.

It is well known that the shapes and positions of the amide I (1700–1600 cm^{-1}) and amide II (1600–1500 cm^{-1}) infrared transmission bands of proteins can provide detailed information on the secondary structure of polypeptide chain of the proteins (Kauppinen et al., 1981). FTIR spectra of dry Hb and Hb-NBTSMs composite films (Fig. S7) showed that the spectra of amide I and II bands of Hb in Hb-NBTSMs composite film (1650 and 1538 cm^{-1}) were nearly the same as those obtained for native Hb (1653 and 1540 cm^{-1}). The similarities of the two spectra further also suggested that the Hb retained the essential feature of its native secondary structure in the NBTSMs film and had good biocompatibility with the NBTSMs. The good biocompability of Hb entrapped in the NBTSMs could perhaps be attributed to its rigid framework and high chemical activity, which was available to hide or bind Hb and thus restrained its conformational change and unfolding.

3.4. Direct electrochemical property of the film electrodes

Fig. 4A shows cyclic voltammograms of different modified electrodes in PBS at 0.2 V s^{-1}. No peak was observed (curve a) at the NBTSMs electrode, showing that the NBTSMs were not an electroactive material in the potential range. However, the Hb-NBTSMs

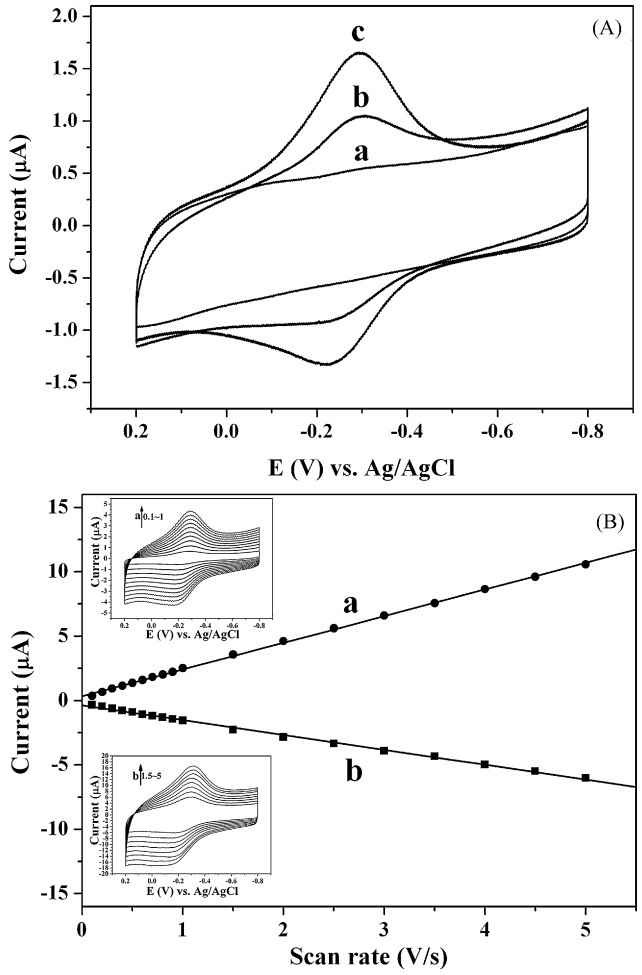

Fig. 4. (A) Cyclic voltammograms of (a) NBTSMs, (b) Hb-Chi-NBTSMs, and (c) Hb-NBTSMs electrodes in PBS with the scan rate of 0.2 V s^{-1}. (B) Plots of oxidation peak currents and reduction peak currents versus scan rates for the Hb-NBTSMs electrode. Scan rates: 0.1, 0.2, 0.3, 0.4, 0.5, 0.6, 0.7, 0.8, 0.9, 1.0 V s^{-1} (inset a) and 1.5, 2.0, 2.5, 3.0, 3.5, 4.0, 4.5, 5.0 V s^{-1} (inset b).

electrode exhibited a couple of nearly reversible and well-defined peaks (curve c), which could be attributed to the direct electron transfer between the Hb and the underlying electrode (Lu et al., 2008). Interestingly, compared with the Hb-NBTSMs/GC electrode fabricated by the self-assembly strategy, the redox peaks observed at the Hb-Chi-NBTSMs/GC (curve b) that was prepared using a common method, wherein, Chi was used to immobilize Hb and NBTSMs onto the activated GC electrode, were much smaller (less than 3.5-fold). This was probably because the micropores of the activated GC electrode and nanometer-scale cavities among intercalated nanoplates were filled with Chi and thus that the active sites available for electron transfer greatly decreased. Moreover, the lengthened electron transfer path at the Chi-based electrode would weaken the electron transfer capacity, too. The apparent formal potentia $E^{\circ\prime}$ estimated by $(E_{p,a} + E_{p,c})/2$ was about −0.261 V, where $E_{p,a}$ and $E_{p,c}$ are the anodic and cathodic peak potentials, respectively. The $E^{\circ\prime}$ was very close to that (−0.26 V) obtained from the carbonized TiO_2 nanotubes (Guo et al., 2008), and shifted positively than those (e.g., −0.270, −0.286, −0.345 V, etc.) gained from the Hb immobilized on MWNTs/PASE/AuNPs composite (Yang et al., 2008), hollow CdS nanospheres (Dai et al., 2008), and nanosheet-based ZnO microspheres (Lu et al., 2008), respectively. Furthermore, the $E^{\circ\prime}$ shifted negatively 20 mV and even more as compared with that obtained from the MWNTs matrix (Qi et al., 2006) and other matrixes (Salimi et al., 2006; Yang et al., 2007). The studies indicated

that the component and shape of nanomaterials played a decisive role in the formal potential of proteins. The peak-to-peak separation (ΔE_p) was about 60 mV at 0.2 V s^{-1}, which was smaller than those reported for the Hb in Fe_3O_4 nanoparticles (Cao and Hu, 2006) and mesoporous silica matrix (Dai et al., 2004) observed at the same scan rate. Such a smaller ΔE_p value revealed more reversible behavior for faster electron transfer of Hb than those previously reported.

Using Faraday's law, $Q = nFA\Gamma^*$ (Q, n, F, A, and Γ^* represent the quantity of charge, the number of electron transferred, Faraday constant, effective electrode area, and surface average concentration of electroactive enzyme, respectively), the Γ^* of the electroactive Hb in the NBTSMs film was estimated to be about 1.20×10^{-10} mol/cm^2 (assuming a one-electron transfer reaction). The total amount of adsorbed Hb (Γ) was about 4.38×10^{-9} mol cm^{-2}, indicating that the electroactive Hb in the NBTSMs film was about 2.74% of the total Hb content deposited on the electrode. The Γ^* was six times higher than that of the theoretical monolayer coverage (about 1.9×10^{-11} mol cm^{-2}) (Wang, 2005). This suggested that six layers of the self-assembly Hb molecules closest to the electrode participated in transferring electrons to the underlying electrode, which could be ascribed to the following advantages. First, NBTSMs possessed plentiful oxygen vacancies and thus had good electron transfer carrier. Second, any cross-linking reagents (e.g., chitosan, ferrocene derivatives, nafion, etc.), which, to some extent, possibly restrain electron transfer between enzymes and underlying electrodes, were not used. Third, the intercalated structure among the nanoplates resulted in numerous nanometer-scale cavities and highly active sites, which may be available to bind Hb and provide an efficient electron-conducting tunnel. Finally, the sub-microspheres, served as a rigid framework, could hide Hb and thus restrained its conformational change and unfolding for favoring the appropriate conformation.

Fig. 4B gives representative cyclic voltammograms of the Hb-NBTSMs electrode scanned at low and high scan rates, respectively. It can be seen that both the reduction and oxidation peak currents increased linearly with increasing scan rates up to 5 V s^{-1}, indicating that all of the electroactive Hb in the film were reduced on the forwarded cathodic scan and the reduced Hb was then converted to the oxidized form on the reverse anodic scan. This result indicated that the NBTSMs provided a friendly microenvironment for the intercalated Hb to maintain its activity to a great extent and it was a surface-confined electrochemical process. The kinetic parameter k_s of the Hb immobilized on the NBTSMs modified electrode was estimated using the model of Laviron (Laviron, 1974):

$$\log k_s/s^{-1} = \alpha \log(1-\alpha) + (1-\alpha)\log\alpha - \log\left[\frac{RT/nF\upsilon}{s}\right] - \frac{\alpha(1-\alpha)nF\Delta E_p}{2.3RT}$$

where α, k_s, ΔE_p, n, R, T, and υ mean charge transfer coefficient, heterogeneous electron-transfer rate constant, peak separation, the number of electrons transferred, gas constant, absolute temperature, and scan rate, respectively. By taking α as 0.5 and $\upsilon > 0.2$ V s^{-1}, the average k_s was determined to be 20.0 ± 3.8 s^{-1}, which was much larger than those at the reported CNTs (1.16 s^{-1}) and BCNTs (1.56 s^{-1}) modified electrodes (Deng et al., 2008). This implied that the NBTSMs modified electrode facilitated more effectively electron transfer between the redox-active sites of enzyme and the electrode than some commonly nanomaterial-modified electrodes.

The influence of the solution pH on the electrochemistry behavior of Hb at the Hb-NBTSMs electrode was also evaluated. Fig. 5 gives cyclic voltammograms of the Hb-NBTSMs electrode in the solutions with different pH values. Stable and well-defined cyclic voltammograms could be observed in the pH range of 4.0–8.0. With increasing pH from 4.0 to 8.0, both the reduction and oxidation peaks shifted

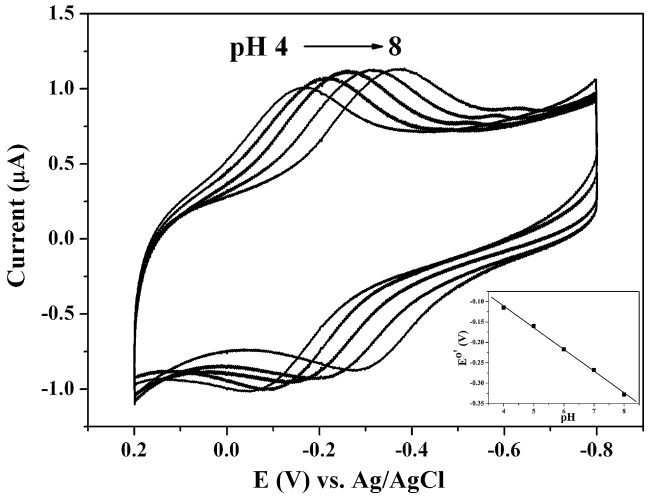

Fig. 5. Cyclic voltammograms of the Hb-NBTSMs electrode with pH values of 4.0, 5.0, 6.0, 7.0, and 8.0 (from left to right). Inset: plot of the apparent formal potentials versus pH values. Scan rate: 0.2 V s^{-1}.

linearly to the negative (the inset of Fig. 5). All these voltammetric peak potentials switched among pH values were reversible. The slope from the linear plot of $E^{\circ\prime}$ versus pH was about −53.4 mV/pH, which was close to the theoretical value of −58.0 mV/pH for a single proton transfer coupled to a reversible single electron transfer. Therefore, the reaction could be represented as follows:

$$Hb[Heme(Fe^{III})] + H^+ + e^- \rightarrow Hb[Heme(Fe^{II})]$$

3.5. Electrocatalytic property of the Hb-NBTSMs/GC electrode

As one of the most extensively studied proteins, Hb plays a critical biological role in many fields such as biosensing, biocatalysis, and biodetection because bioactive hemoglobin immobilized on an electrode surface usually exhibits good electrocatalytic activity for oxygen, hydrogen peroxide, trichloroacetic acid, nitrite, etc. (Huang et al., 2002). In the biosensing system, electrocatalytic property of the Hb-NBTSMs/GC electrode was studied through taking H_2O_2 as a model. When H_2O_2 was added to PBS, the voltammograms of the Hb-NBTSMs/GC electrode showed a significant increase in the reduction peak current at about −0.30 V with the disappearance of the oxidation peak current (Fig. 6A), suggesting that an electrocatalytic reduction of H_2O_2 occurred. The reduction peak current increased with increasing H_2O_2 concentration. However, there were no peaks observed at the NBTSMs/GC electrode in a potential range of 0.2 to −0.8 V in the presence of H_2O_2, indicating that the NBTSMs/GC electrode did not possess electrocatalytic capacity towards H_2O_2. The possible mechanism of electrocatalytic reduction of H_2O_2 should be similar to that reported recently (Lu et al., 2008), which could be expressed as follows:

$$Hb[Heme(Fe^{III})] + H_2O_2 \rightarrow \text{compoundI} + H_2O \quad (1)$$

$$\text{CompoundI} + H_2O_2 \rightarrow Hb[Heme(Fe^{III})] + H_2O + O_2 \quad (2)$$

$$Hb[Heme(Fe^{III})] + H^+ + e^- \rightarrow Hb[Heme(Fe^{II})] \quad \text{at electrode} \quad (3)$$

$$Hb[Heme(Fe^{II})] + O_2 \rightarrow Hb[Heme(Fe^{II})]\text{–}O_2 \quad \text{fast} \quad (4)$$

$$Hb[Heme(Fe^{II})]\text{-}O_2 + H^+ + e^- \rightarrow Hb[Heme(Fe^{III})] + H_2O_2 \quad \text{at electrode} \quad (5)$$

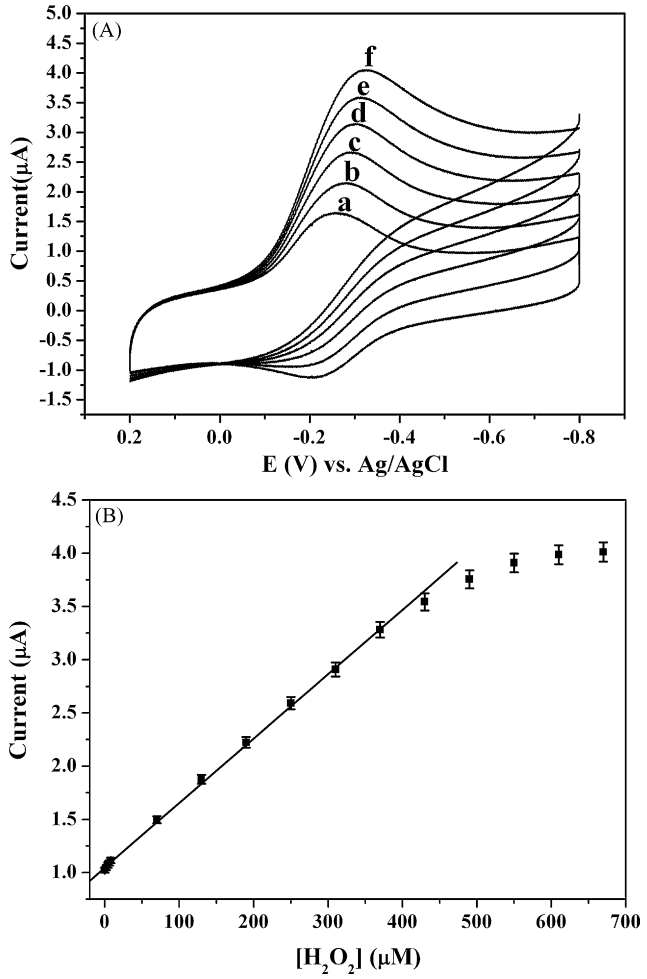

Fig. 6. (A) Bioelectrocatalysis of the biosensor towards H_2O_2 in PBS with the scan rate of 0.2 V s^{-1} and H_2O_2 concentrations of (a) 0, (b) 60, (c) 120, (d) 180, (e) 240, and (f) 300 μM. (B) Plot of electrocatalytic currents (I_{cat}) versus H_2O_2 concentrations for the Hb-NBTSMs/GC electrode in PBS.

The overall reaction of (1–5) would be:

$$H_2O_2 + 2H^+ + 2e^- \rightarrow 2H_2O \quad (6)$$

As shown in Fig. 6B, the cathodic reduction currents increased linearly with increasing H_2O_2 concentrations and the linear range was from 2.0×10^{-6} to 4.3×10^{-4} M ($R = 0.9999$, $n = 11$), which was much wider than the reported value (Lu et al., 2008). The detection limit of H_2O_2 at the Hb-NBTSMs electrode was 4.6×10^{-7} M when signal-to-noise ratio (S/N) was 3. The sensitivity of the enzyme electrode was calculated to be about 84 mA cm^{-2} M^{-1}, indicating a good bioelectrocatalytic activity towards H_2O_2.

At higher H_2O_2 concentrations, the plot tended to level off, which was characteristic of enzyme-based catalysis. The apparent Michaelis–Menton constant (K_M^{app}) could be estimated according to the Lineweaver–Burk equation (Kamin and Wilson, 1980):

$$I_{ss}^{-1} = I_{max}^{-1} + K_M^{app} C^{-1} I_{max}^{-1}$$

where I_{ss}, I_{max}, and C stand for the steady-state response current after the addition of substrate, the maximum current measured under saturated substrate condition, and the bulk concentration of the substrate. In this biosensing system, K_M^{app} was estimated to be about 204 μM, which was smaller than those reported (Yang et al., 2007; Xu et al., 2007b). The relatively small K_M^{app} indicated that the Hb-NBTSMs/GC electrode had high catalytic efficiency to the reduction of H_2O_2.

3.6. Reproducibility and stability of the biosensor

The reproducibility of the biosensor was evaluated at a given concentration in the linear range by cyclic voltammetric measurements. The relative standard deviation (R.S.D.) of the biosensor response to 60 μM H_2O_2 for 6 successive measurements was 2.6%, indicating a good reproducibility. To evaluate electrode-to-electrode reproducibility, three biosensors were prepared under the same and independent conditions. The R.S.D. of the biosensors was 3.1%, indicating a good electrode-to-electrode reproducibility.

The stability of the biosensor was studied by comparing the cyclic voltammetric peak currents of the Hb entrapped in the NBTSMs with time intervals of 4 h. The decrease of the cathodic peak current of the biosensor immersed in PBS for 4 h was less than 1.7%, indicating that the biosensor possessed a good stability. Moreover, the biosensor could retain 96.4% of its initial response after 20-day storage, suggesting a good long-term stability. Of particular mention here is the fabrication of our biosensor without using any cross-linking reagents, so the reproducibility and stability of the biosensor were desirable and satisfying. The good reproducibility and stability can be ascribed to the unique microstructure, shape and good biocompatibility of the NBTSMs.

4. Conclusion

Nanoplated bismuth titanate sub-microspheres constructed with tens of $Bi_4Ti_3O_{12}$ nanoplates were synthesized by a facile hydrothermal synthesis strategy. The sub-microspheres with plenteous oxygen atoms and highly active sites were explored for the construct of direct electrochemical biosensor through a combined hydrogen bond and electrostatic assembly process, and have also been proved to be a good matrix for protein immobilization and electrochemical biosensor construction. With advantages of the $Bi_4Ti_3O_{12}$ inorganic material, enhanced direct electron transfer and good biocatalytic activity could be easily obtained through entrapping metalloenzymes into the $Bi_4Ti_3O_{12}$-based composite material. These results revealed that Hb entrapped in the composite film retained its essential secondary structure and the NBTSMs-based biosensor displayed good electrochemical performance such as a wide linear range, low detection limit, good reproducibility and stability, and good long-term stability for the detection of H_2O_2. The nanoplate-constructed $Bi_4Ti_3O_{12}$ sub-microspheres are also expected to find potential applications in biomedical, food, and environmental analysis and detection.

Acknowledgement

The work was supported by National Natural Science Foundation of China (nos. 20773040 and 50702022).

Appendix A. Supplementary data

Supplementary data associated with this article can be found, in the online version, at doi:10.1016/j.bios.2009.04.037.

References

Armstrong, F.A., Hill, H.A.O., Walton, N.J., 1988. Acc. Chem. Res. 21, 407–413.
Cai, W.Y., Feng, L.D., Liu, S.H., Zhu, J.J., 2008. Adv. Funct. Mater. 18, 3127–3136.
Cao, D.F., Hu, N.F., 2006. Biophys. Chem. 121, 209–217.
Chen, X., Fu, C.L., Wang, Y., Yang, W.S., Evans, D.G., 2008. Biosens. Bioelectron. 24, 356–361.
Cheng, G.F., Zhao, J., Tu, Y.H., He, P.G., Fang, Y.Z., 2005. Anal. Chim. Acta 533, 11–16.
Dai, Z.H., Bai, H.Y., Hong, M., Zhu, Y.Y., Bao, J.C., Shen, J., 2008. Biosens. Bioelectron. 23, 1869–1873.
Dai, Z.H., Liu, S.Q., Ju, H.X., Chen, H.Y., 2004. Biosens. Bioelectron. 19, 861–867.
Deng, C.Y., Chen, J.H., Chen, X.L., Xiao, C.H., Nie, L.H., Yao, S.Z., 2008. Biosens. Bioelectron. 23, 1272–1277.

Di, J.W., Peng, S.H., Shen, C.P., Gao, Y.S., Tu, Y.F., 2007. Biosens. Bioelectron. 23, 88–94.
Du, D., Huang, X., Cai, J., Zhang, A.D., 2007. Sens. Actuators B 127, 531–535.
Guo, C.X., Hu, F.P., Li, C.M., Shen, P.K., 2008. Biosens. Bioelectron. 24, 819–824.
Heller, A., 1990. Acc. Chem. Res. 23, 128–134.
Huang, H., Hu, N.F., Zeng, Y.H., Zhou, G., 2002. Anal. Biochem. 308, 141–151.
Ivnitski, D., Branch, B., Atanassov, P., Apblett, C., 2006. Electrochem. Commun. 8, 1204–1210.
Jia, J.B., Wang, B.Q., Wu, A.G., Cheng, G.J., Li, Z., Dong, S.J., 2002. Anal. Chem. 74, 2217–2223.
Kamin, R.A., Wilson, G.S., 1980. Anal. Chem. 52, 1198–1205.
Kauppinen, J.K., Moffate, D.J., Mantsch, H.H., Lameron, D.G., 1981. Appl. Spectrosc. 35, 271–276.
Laviron, E., 1974. J. Electroanal. Chem. 52, 355–393.
Li, J.W., Fan, C., Xiao, F., Yan, R., Fan, S.S., Zhao, F.Q., Zeng, B.Z., 2007. Electrochim. Acta 52, 6178–6185.
Liu, Y., Wang, M.K., Zhao, F., Xu, Z.A., Dong, S.J., 2005. Biosens. Bioelectron. 21, 984–988.
Lu, X.B., Zhang, H.J., Ni, Y.W., Zhang, Q., Chen, J.P., 2008. Biosens. Bioelectron. 24, 93–98.
Nagaoka, T., Yoshino, T., 1986. Anal. Chem. 58, 1037–1042.
Pal, S., Alocilja, E.C., Downes, F.P., 2007. Biosens. Bioelectron. 22, 2329–2336.
Pei, R.J., Cheng, Z.L., Wang, E.K., Yang, X.R., 2001. Biosens. Bioelectron. 16, 355–361.
Qi, H.L., Zhang, C.X., Li, X.R., 2006. Sens. Actuators B Chem. 114, 364–370.
Qiao, Y.B., Jian, F.F., Bai, Q., 2008. Biosens. Bioelectron. 23, 1244–1249.
Rinehart, J.P., Li, A.Q., Yocum, G.D., Robich, R.M., Hayward, S.A.L., Denlinger, D.L., 2007. Proc. Natl. Acad. Sci. U.S.A. 104, 1130–1137.
Salimi, A., Sharifi, E., Noorbakhsh, A., Soltanian, S., 2006. Electrochem. Commun. 8, 1499–1508.
Shi, K., Hu, K., Wang, S., Lau, C.Y., Shiu, K.K., 2007. Electrochim. Acta 52, 5907–5913.
Villegas, M., Moure, C., Fernandez, J.F., Duran, P., 1996. Ceram. Int. 22, 15–22.
Wang, J., 2008. Chem. Rev. 108, 814–825.
Wang, F., Chen, X.X., Xu, Y.X., Hu, S.S., Gao, Z.N., 2007. Biosens. Bioelectron. 23, 176–182.
Wang, J., 2005. Analyst 130, 421–426.
Wang, H.S., Ju, H.X., Chen, H.Y., 2002. Electroanalysis 14, 1615–1620.
Willner, I., Willner, B., Katz, E., 2007. Bioelectrochemistry 70, 2–11.
Xu, J.M., Li, W., Yin, Q.F., Zhong, H., Zhu, Y.L., Jin, L.T., 2007b. J. Colloid Interface Sci. 315, 170–176.
Xu, S.Y., Peng, B., Han, X.Z., 2007a. Biosens. Bioelectron. 22, 1807–1810.
Yang, J., Pang, F.Y., Zhang, R.Y., Xu, Y., He, P.G., Fang, Y.Z., 2008. Electroanalysis 20, 2134–2140.
Yang, M.H., Qu, F.L., Li, Y.J., He, Y., Shen, G.L., Yu, R.Q., 2007. Biosens. Bioelectron. 23, 414–420.
Yang, Q.B., Li, Y.X., Yin, Q.R., Wang, P.L., Cheng, Y.B., 2003. J. Eur. Ceram. Soc. 23, 161–166.
Zhang, L., Zhang, Q., Li, J.H., 2007. Adv. Funct. Mater. 17, 1958–1965.
Zhang, J.D., Oyama, M., 2005. J. Electroanal. Chem. 577, 273–279.